GEOPHYSICS, VOL. 66, NO. 3 (MAY-JUNE 2001); P. 883–889, 12 FIGS., 1 TABLE.

3-D traveltime computation using Huygens wavefront tracing

Paul Sava* and Sergey Fomel*

ABSTRACT

Traveltime computation is widely used in seismic modeling, imaging, and velocity analysis. The two most commonly used methods are ray tracing and numerical solutions to the eikonal equation. Eikonal solvers are fast and robust but are limited to computing only the first-arrival traveltimes. Ray tracing can compute multiple arrivals but lacks the robustness of eikonal solvers. We propose a robust and complete method of traveltime computation. It is based on a system of partial differential equations, which is equivalent to the eikonal equation but formulated in the ray-coordinates system. We use a first-order discretization scheme that is interpreted very simply in terms of the Huygens's principle. Our explicit finite-difference solution to the eikonal equation solved in the ray-coordinates system delivers both computational speed and stability since we use more than one point on the current wavefront at every time step. The finite-difference method has proven to be a robust alternative to conventional ray tracing, while being faster and having a better ability to handle rough velocity media and penetrate shadow zones.

INTRODUCTION

Though traveltime computation is widely used in seismic modeling and imaging, attaining sufficient accuracy without compromising speed and robustness is often a problem. Moreover, there is no easy way to obtain the traveltimes corresponding to the multiple arrivals that appear in complex velocity media.

The trade-off between speed and accuracy becomes apparent in the choice between the two most commonly used methods: ray tracing and numerical solutions to the eikonal equation. Other methods reported in the literature—for example, dynamic programming (Moser, 1991) and wavefront construction (Vinje et al., 1993)—are less common in practice (Audebert et al., 1997).

Eikonal solvers provide a relatively fast and robust method of traveltime computations (Vidale, 1990; van Trier and Symes, 1991; Sethian and Popovici, 1999). They also avoid the problem of traveltime interpolation to a regular grid, which imaging applications require. However, the conventional eikonal solvers compute first-arrival traveltimes and lack the important ability to track multiple arrivals. In complex velocity structures, the first arrivals do not necessarily correspond to the most energetic waves, and other arrivals can be crucially important for accurate modeling and imaging (Geoltrain and Brac, 1993; Gray and May, 1994).

On the other hand, one-point ray tracing can compute multiple arrivals with great accuracy. Unfortunately, it lacks the robustness of eikonal solvers. Increasing the accuracy of ray tracing in the regions of complex velocity variations raises the cost of the method and makes it prohibitively expensive for routine large-scale applications. Mathematically, ray tracing amounts to a numerical solution of the initial value problem for a system of ordinary differential equations (Červený, 1987). These ray equations describe characteristic lines of the eikonal partial differential equation.

Here, we propose a different approach to traveltime computation. It is robust and has the ability to find multiple arrival traveltimes. The theoretical construction is based on a system of partial differential equations, equivalent to the eikonal equation but formulated in the ray-coordinates system. Unlike eikonal solvers, our method produces the output in ray coordinates. Unlike ray tracing, it is computed by a numerical solution of partial differential equations. We show that the first-order discretization scheme has a remarkably simple interpretation in terms of the Huygens's principle, and we propose a Huygens wavefront tracing (HWT) scheme as a robust alternative to conventional ray tracing. Numerical examples demonstrate the method's stability in media with strong and sharp lateral velocity variations, better coverage of shadow zones, and increased speed compared with paraxial ray tracing.

Manuscript received by the Editor June 21, 1999; revised manuscript received June 5, 2000.
*Stanford University, Stanford Exploration Project, Department of Geophysics, Stanford, California. E-mail: paul@sep.stanford.edu; sergey@sep.stanford.edu.
© 2001 Society of Exploration Geophysicists. All rights reserved.

CONTINUOUS THEORY

The 3-D eikonal equation, governing the traveltimes from a fixed source in isotropic heterogeneous media, has the form

$$\left(\frac{\partial\tau}{\partial x}\right)^2+\left(\frac{\partial\tau}{\partial y}\right)^2+\left(\frac{\partial\tau}{\partial z}\right)^2=\frac{1}{v^2(x,y,z)}. \qquad (1)$$

Here x, y, and z are spatial coordinates, τ is the traveltime (eikonal), and v is the velocity field. Constant-traveltime surfaces in the traveltime field $\tau(x,y,z)$, constrained by equation (1) and appropriate boundary conditions, correspond to wavefronts of the propagating wave. Additionally, each point on a wavefront can be parameterized by two arbitrarily chosen ray parameters γ and ϕ.

For a point source, γ and ϕ can be chosen as the initial ray angles at the source. Zhang (1993) shows that γ and ϕ as a function of spatial coordinates satisfy the simple partial differential equations

$$\frac{\partial\tau}{\partial x}\frac{\partial\gamma}{\partial x}+\frac{\partial\tau}{\partial y}\frac{\partial\gamma}{\partial y}+\frac{\partial\tau}{\partial z}\frac{\partial\gamma}{\partial z}=0$$

and

$$\frac{\partial\tau}{\partial x}\frac{\partial\phi}{\partial x}+\frac{\partial\tau}{\partial y}\frac{\partial\phi}{\partial y}+\frac{\partial\tau}{\partial z}\frac{\partial\phi}{\partial z}=0. \qquad (2)$$

Equations (2) merely express the fact that in an isotropic medium, rays are locally orthogonal to wavefronts.

It is important to note that for complex velocity fields, τ, γ, and ϕ as functions of x, y, and z become multivalued (Figure 1). In this case, the multivalued character of the ray parameters, γ and ϕ, corresponds to the situation where more than one ray from the source passes through a particular point $\{x,y,z\}$ in the subsurface. This situation presents a very difficult problem when equations (1) and (2) are solved numerically. Typically, only the first-arrival branch of the traveltime is picked in the numerical calculation. The ray-tracing method is free from that limitation because it operates in the ray-coordinates system. Ray tracing computes the traveltime τ and the corresponding ray positions x, y, z for a fixed pair of ray parameters (γ and ϕ).

Since $x(\tau,\gamma,\phi)$, $y(\tau,\gamma,\phi)$, and $z(\tau,\gamma,\phi)$ are uniquely defined for arbitrarily complex velocity fields, we can now make the following mathematical transformation. Considering equations (1) and (2) as a system and applying the general rules of calculus, we can transform this system by substituting the inverse functions $x(\tau,\gamma,\phi)$, $y(\tau,\gamma,\phi)$, and $z(\tau,\gamma,\phi)$ for the original fields τ, γ, and ϕ. The resultant expressions take the form

$$\left(\frac{\partial x}{\partial\tau}\right)^2+\left(\frac{\partial y}{\partial\tau}\right)^2+\left(\frac{\partial z}{\partial\tau}\right)^2=v^2(x,y,z) \qquad (3)$$

and

$$\begin{aligned}\frac{\partial x}{\partial\tau}\frac{\partial x}{\partial\gamma}+\frac{\partial y}{\partial\tau}\frac{\partial y}{\partial\gamma}+\frac{\partial z}{\partial\tau}\frac{\partial z}{\partial\gamma}&=0,\\ \frac{\partial x}{\partial\tau}\frac{\partial x}{\partial\phi}+\frac{\partial y}{\partial\tau}\frac{\partial y}{\partial\phi}+\frac{\partial z}{\partial\tau}\frac{\partial z}{\partial\phi}&=0.\end{aligned} \qquad (4)$$

Comparing equations (3) and (4) with the original system [equations (1)–(2)] shows that equations (3) and (4) again represent the dependence of ray coordinates and Cartesian coordinates in the form of partial differential equations. However, the solutions of the second system [equations (3)–(4)] are better behaved and have a unique value for every τ, γ, and ϕ. We could also compute these values with conventional ray tracing. However, the ray-tracing approach is based on a system of ordinary differential equations, which represents a very different mathematical model.

We use equations (3) and (4) as the basis of our wavefront tracing algorithm. The next section discusses the discretization of the partial differential equations and the physical interpretation we have given to the scheme.

DISCRETIZATION SCHEME AND THE HUYGENS'S PRINCIPLE

A natural first-order discretization scheme for equation (3) leads to the difference equation

$$\left(x^{i,k}_{j+1}-x^{i,k}_{j}\right)^2+\left(y^{i,k}_{j+1}-y^{i,k}_{j}\right)^2+\left(z^{i,k}_{j+1}-z^{i,k}_{j}\right)^2=\left(r^{i,k}_{j}\right)^2, \qquad (5)$$

where the index i corresponds to the ray parameter γ, k corresponds to the ray parameter ϕ, j corresponds to the traveltime τ, $r^{i,k}_j=\triangle\tau\, v^{i,k}_j$, $\triangle\tau$ is the increment in time, and $v^{i,k}_j$ is the velocity at the $\{i,k,j\}$ grid point. Equation (5) describes a sphere with the center at $\{x^{i,k}_j, y^{i,k}_j, z^{i,k}_j\}$ and the radius $r^{i,k}_j$. This sphere is, of course, the wavefront of a secondary Huygens source.

This observation suggests that we apply the Huygens's principle directly to find an appropriate discretization for equation (4). Let us consider a family of Huygens spheres, centered at the points along the current wavefront (τ). Mathematically, this family is described by an equation analogous to equation (5) as follows:

$$[x-x(\gamma,\phi)]^2+[y-y(\gamma,\phi)]^2+[z-z(\gamma,\phi)]^2=r^2(\gamma,\phi). \qquad (6)$$

Here the ray parameters γ and ϕ serve as the parameters that distinguish a particular Huygens source. According to the Huygens's principle, the next wavefront corresponds to the envelope of the wavefront family. To find the envelope condition, we can differentiate both sides of equation (6) with respect to the family parameter, γ or ϕ.

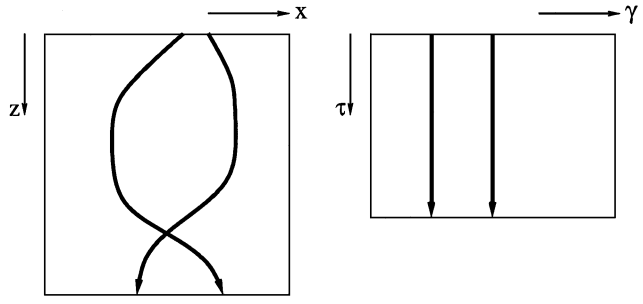


FIG. 1. A comparison of ray representation in Cartesian and ray coordinates. The ray coordinates expressed as functions of the Cartesian coordinates are multivalued (left). On the contrary, the Cartesian coordinates expressed as functions of the ray coordinates are single valued (right).

To complete the discretization, we can represent the γ and ϕ derivatives by a centered finite-difference approximation. This representation yields the scheme

$$\begin{aligned}&\left(x_j^{i,k}-x_{j+1}^{i,k}\right)\left(x_j^{i+1,k}-x_j^{i-1,k}\right)\\&\quad+\left(y_j^{i,k}-y_{j+1}^{i,k}\right)\left(y_j^{i+1,k}-y_j^{i-1,k}\right)\\&\quad+\left(z_j^{i,k}-z_{j+1}^{i,k}\right)\left(z_j^{i+1,k}-z_j^{i-1,k}\right)=r_j^{i,k}\left(r_j^{i+1,k}-r_j^{i-1,k}\right)\end{aligned}\tag{7}$$

and

$$\begin{aligned}&\left(x_j^{i,k}-x_{j+1}^{i,k}\right)\left(x_j^{i,k+1}-x_j^{i,k-1}\right)\\&\quad+\left(y_j^{i,k}-y_{j+1}^{i,k}\right)\left(y_j^{i,k+1}-y_j^{i,k-1}\right)\\&\quad+\left(z_j^{i,k}-z_{j+1}^{i,k}\right)\left(z_j^{i,k+1}-z_j^{i,k-1}\right)=r_j^{i,k}\left(r_j^{i,k+1}-r_j^{i,k-1}\right),\end{aligned}\tag{8}$$

which supplements the previously found scheme [equation (5)] for a unique determination of the point $\{x_{j+1}^i, y_{j+1}^i, z_{j+1}^i\}$ on the (i,k)th ray and the $(j+1)$th wavefront.

Formulas (5), (7), and (8) define the update scheme for the finite-difference algorithm, and Figures 2 and 4 present their geometrical interpretation.

To fill the $\{\tau,\gamma,\phi\}$ volume, the scheme needs to be initialized with one complete wavefront around the wave source and a bundle of boundary rays to account for the exterior of the γ–ϕ domain. This second part of the initialization can be replaced by local wavefront extrapolation, as discussed in the next section.

The solution to the system expressed by equations (5), (7), and (8) has an explicit form. Figure 3 is a plot of the finite-difference stencils for the 2-D and 3-D cases.

BOUNDARIES AND TRIPLICATIONS

This section presents a short discussion of the special treatment required by the boundaries of the computation domain. These boundaries are of two kinds: exterior boundaries, represented by the edges of the computational domain, and interior boundaries, represented by the triplication lines. Because of the centered finite-difference scheme, HWT cannot be used at the boundaries of the computational domain. This means the boundaries need to be treated differently from the rest of the domain. Also, the centered finite-difference scheme cannot be used when the wavefronts create triplications. Triplications represent points of discontinuity of the derivative along the wavefront; therefore, the centered finite-difference representation of the derivative is inappropriate. Figure 5 describes a point of triplication represented in both the physical (Cartesian) domain (left) and the ray-coordinates domain (right).

One possible solution for the boundaries is to make a local approximation of the wavefront. Instead of considering the actual points on the wavefront, we can create an approximate

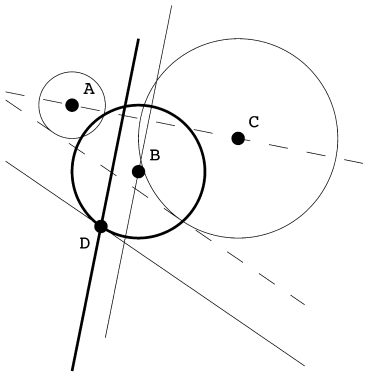


FIG. 2. A geometrical updating scheme for the 2-D HWT in the physical domain. Three points on the current wavefront (A, B, and C) are used to compute the position of the D point. The bold lines represent the 2-D versions of equations (5) and (7). The tangent to circle B at point D is parallel to the common tangent of circles A and C.

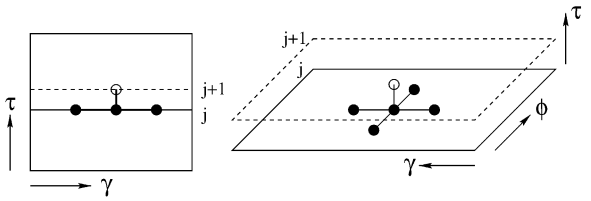


FIG. 3. Finite-difference stencils for HWT. The 2-D stencils consists of three points on the current wavefront (left), while the 3-D case consists of five points on the current wavefront.

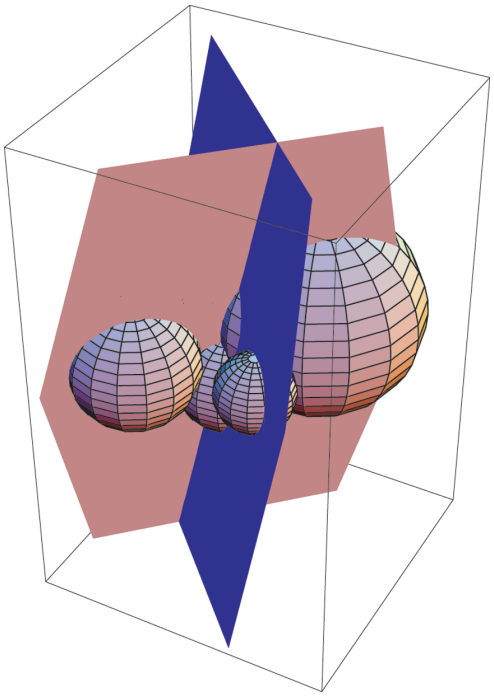


FIG. 4. A geometrical updating scheme for the 3-D HWT in the physical domain. Five points on the current wavefront, represented by the five spheres, not all visible, with radii defined by the velocities at the corresponding points of the wavefront, are used to compute a point on the next wavefront. The sphere in the middle represents equation (5), and the planes represent equations (7) and (8).

wavefront that is locally orthogonal to the ray arriving at the cusp point, as depicted in Figure 6. We can then pick an appropriate number of points (two in two dimensions or four in three dimensions) on this approximate wavefront and use the HWT scheme without any change. A new search for the cusp points is then needed on the new wavefront before we can proceed further.

The flowchart in Figure 7 summarizes the algorithm.

EXAMPLES

This section presents three examples of traveltime computation using HWT. In the first example, we consider a velocity medium with a constant vertical gradient. Figure 8 shows the traveltimes computed using HWT (dotted line) superimposed on the traveltimes obtained using analytical formulas (solid line). The maximum difference is $<0.2\%$.

Next, we present the results of traveltime computation using a complex velocity model that exemplifies the main features of the method. We compare the results of our traveltime computation method with those of full wave-equation modeling for the 2-D salt dome model shown in Figure 9. Figure 10 is a snapshot of the wavefield at 1.23 s, superimposed on an outline of the velocity model. Figure 9 shows, in addition, the wavefront corresponding to the same propagation time (1.23 s) and some of the rays derived from the computed wavefronts.

The first arrivals of the wavefronts superimpose well on the similar events in the wavefield. The later arrivals also superimpose well on the corresponding events in the wavefield, although the sampling is occasionally sparser. This is understandable since in HWT the wavefronts are sampled evenly in the ray domain but not in the physical domain. Because sampling in the two domains is related, a better sampling in the ray domain can generate more accurate sampling in the physical domain. However, sampling is dependent on the model; there is no guarantee of more accurate sampling for rays shot with a smaller angle step. A better idea might be to modify the sampling on the wavefronts dynamically as is done in some of the wavefront construction methods (Vinje et al., 1993).

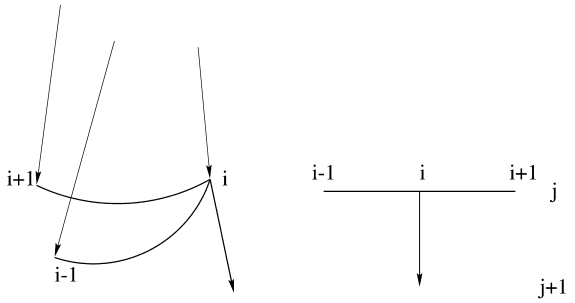


FIG. 5. The centered finite-difference representation of the derivative along the wavefront cannot be used at the cusps. These points represent discontinuities in the derivative and need to be treated separately.

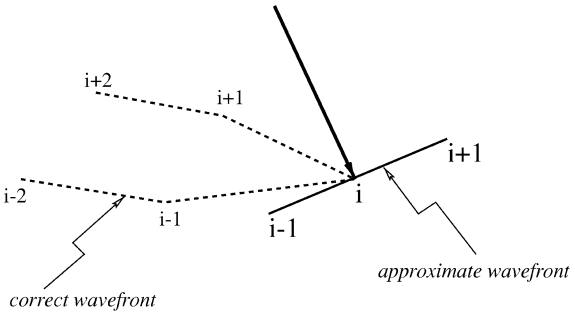


FIG. 6. The centered finite-difference representation of the derivative along the wavefront cannot be used at the cusps. Instead, we can use a local approximation of the wavefront as a plane locally orthogonal to the ray arriving at the cusp.

Finally, we include an example using the 3-D SEG-EAGE salt model. We compare the results obtained using HWT with those obtained using a first-arrival eikonal solver. We present, in both cases, a traveltime cube obtained for a shotpoint located at the surface and at 6000 m in the in-line direction and 8000 m in the cross-line directions.

Figure 11 is the result obtained using the first-arrival eikonal solver. Since the source is located exactly above the salt body, the first arrival is given by the low-energy head waves. However, using Huygens wavefront tracing, we can also obtain some of the later arrivals, from which we can select the one corresponding to the shortest raypath (Figure 12), which is typically equivalent to the most energetic arrival (Nichols et al., 1998).

DISCUSSION

This section briefly compares Huygens wavefront tracing with the other major traveltime computation methods: paraxial ray tracing (Červený, 1987), eikonal solvers (Vidale, 1990; van Trier and Symes, 1991; Qin et al., 1992; Sethian and Popovici, 1999), and wavefront construction (Vinje et al., 1993) (Table 1).

HWT has its output in ray coordinates, the same domain as paraxial ray tracing. However, the latter is done by solving a system of ordinary differential equations in the physical domain, while in HWT the solution is obtained by solving a system of partial differential equations using finite differences in the ray-coordinates domain. The different mathematical model, partial versus ordinary differential equations, makes HWT a better approximation of the wave equation. The reason is that in HWT we include in the computation the partial derivatives along the wavefronts. Therefore, our computations are not based on just one point but spread across a number of neighboring points on the wavefront, which leads to smoother behavior, especially in rough velocity media (Figure 9).

Both HWT and eikonal solvers are finite-difference methods. However, HWT represents a finite-difference method in the ray-coordinates domain while the eikonal solvers represent finite-difference methods in the Cartesian domain. Furthermore, HWT generates all the arrivals, while the eikonal solvers generate only one arrival, typically the first. An explicit finite-difference scheme in ray coordinates is as fast as an explicit finite-difference scheme in Cartesian coordinates. However, with HWT we gain the ability to track multiple arrivals, although at the expense of possibly having to interpolate the traveltimes from one domain to another. Still, in comparison to the fast marching method (Sethian and Popovici, 1999), HWT is simpler because we follow the wavefronts explicitly and we avoid the need to sort the traveltimes along the wavefronts.

HWT is similar to wavefront construction in that both compute each wavefront from the preceding one. However, wavefront construction involves ray tracing from one wavefront to

the next, while in HWT one wavefront is generated from the preceding by finite differences in the ray-coordinates domain.

Finally, HWT is not equivalent to a two-point ray-tracing method (Pereyra, 1992; Strahilevitz et al., 1998) since it creates the traveltimes associated with a given source point. However, it can be adapted to problems that require two-point traveltimes, like traveltime tomography, by using an appropriate ray-matching algorithm.

CONCLUSION

We have presented a finite-difference method of traveltime computation based on a system of differential equations equivalent to the eikonal equation but formulated in the ray-coordinates system. We used a first-order discretization scheme, interpreted very simply in terms of the Huygens's principle. The results obtained so far enable us to the draw the following conclusions.

Stability.—The HWT method is more stable in rough velocity media than the paraxial ray-tracing method. The increased stability results from the fact that HWT derives the points on the new wavefronts from five points on the preceding wavefront, compared to only one in the usual paraxial ray tracing method, which also means that a certain degree of smoothing of the velocity model is already embedded in the method. This feature allows us to use the HWT method in media of very sharp velocity variation and still obtain results that are reasonable from a geophysical point of view (Figure 9).

Coverage.—Being more stable and giving smoother rays than the paraxial ray-tracing method enables the HWT method

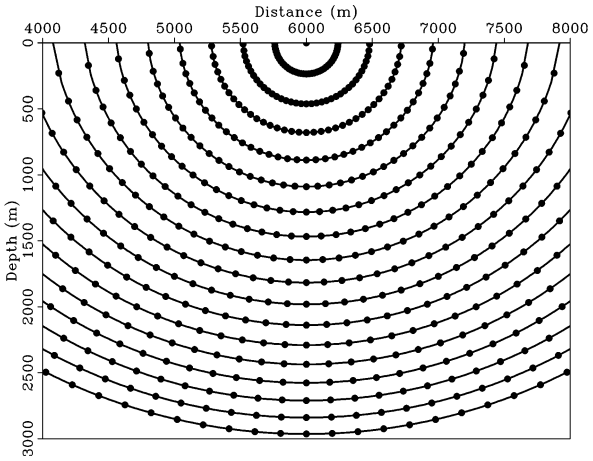


FIG. 8. Constant vertical gradient velocity model example. The thin, solid lines represent the analytical traveltimes, while the thick, dotted line represents the traveltimes computed using HWT.

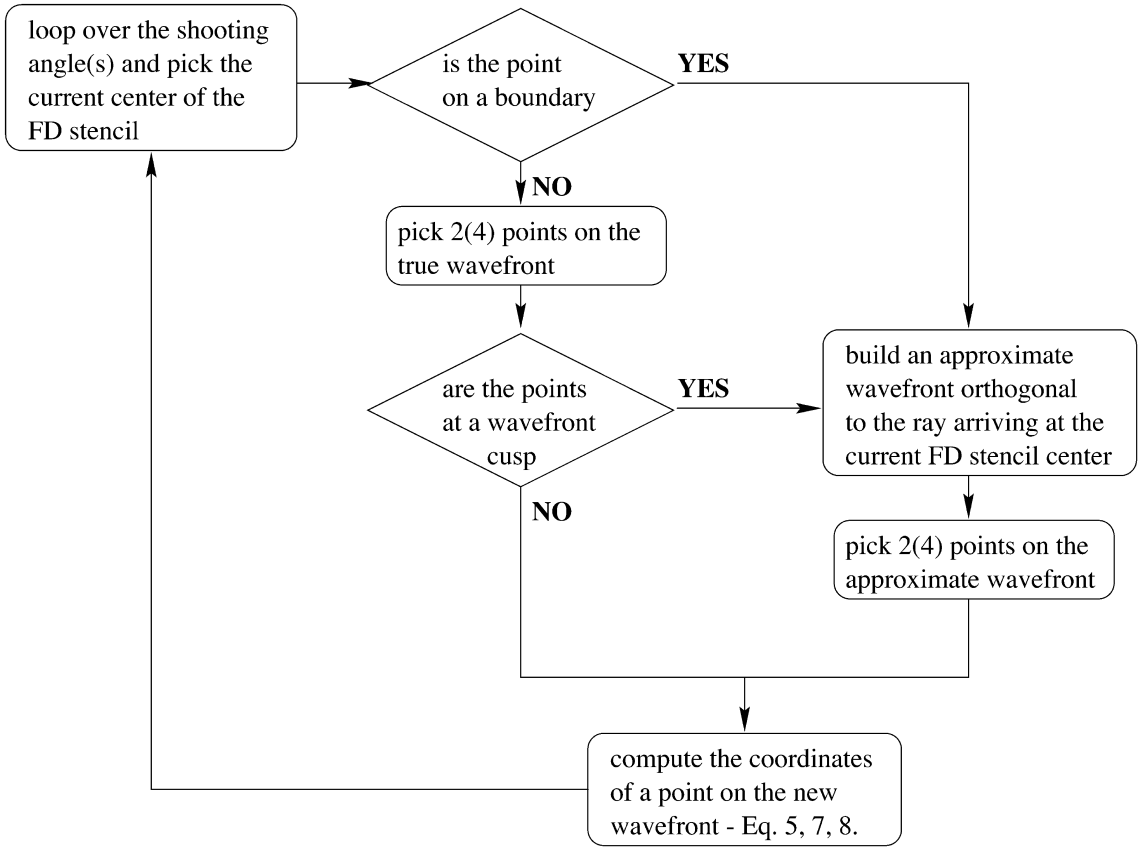


FIG. 7. A flowchart of the HWT algorithm. In two dimensions, the finite-difference stencil is made of three points, while in three dimensions it is made of five points.

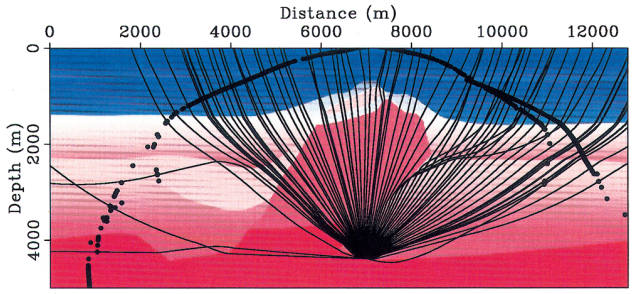


FIG. 9. Rays and one wavefront computed using HWT superimposed on the velocity model. The wavefront was taken at 1.23 s. The velocity model was not smoothed for the traveltime computation.

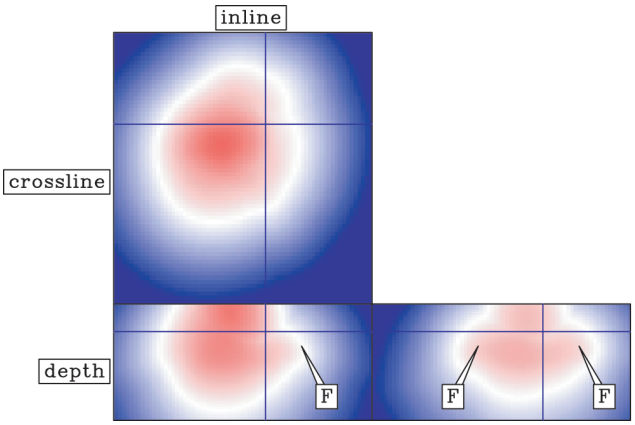


FIG. 11. 3-D SEG-EAGE salt model example. A traveltime cube obtained with a first-arrival eikonal solver. *F* labels the first arrival corresponding to the low-energy head waves.

to provide a better coverage of shadow zones. Moreover, since HWT operates in the ray-coordinates system, it is easy to refine the sampling dynamically along the wavefronts as soon as rays start to diverge.

Speed.—Both HWT and paraxial ray-tracing methods were tested on an SGI Origin 200 computer. In the 2-D case, the execution time for shooting 90 rays of 130 samples for each ray was 1.31 s for the paraxial ray-tracing method and 0.22 s for the HWT method. Also, since HWT operates along the wavefronts, we can dynamically increase or decrease the sampling along the wavefronts, improving the overall speed of the method.

Accuracy.—HWT generates high-accuracy traveltimes, as proven by the examples in this paper (Figures 8 and 10). The accuracy can be improved even further by using a second-order representation of the derivatives along the wavefronts. Also, refining the grid aids both the speed and the accuracy of the method.

The method works in three dimensions and retains all the stability, accuracy, and speed properties of the 2-D version.

ACKNOWLEDGMENTS

We acknowledge ELF Exploration Production for providing us with the salt velocity model we used in this paper.

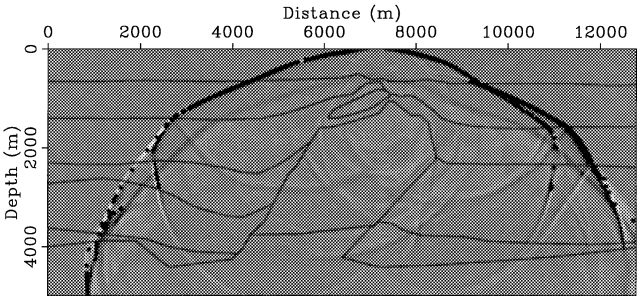


FIG. 10. HWT wavefront superimposed on a wave-equation modeling snapshot at 1.23 s. The portion of the wavefronts corresponding to the first arrival matches well the first arrival of the wavefield. Also, the later HWT arrivals match well the similar events obtained using wave-equation modeling.

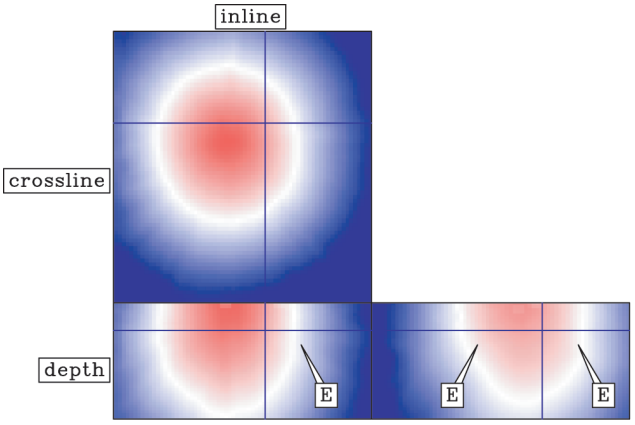


FIG. 12. 3-D SEG-EAGE salt model example. A maximum-energy traveltime cube obtained with Huygens wavefront tracing. *E* labels the most energetic arrival corresponding to the waves traveling directly from the source to the respective location in the subsurface.

Table 1. Comparison of major methods and HWT.

Other major methods	Huygens wavefront tracing (HWT)
One-point ray tracing	
• Finds the solution to a system of ordinary differential equations	• Finds the solution to a system of partial differential equations
Eikonal solvers	
• Give the output in Cartesian coordinates	• Gives the output in ray coordinates
• Compute one arrival	• Computes multiple arrivals
Wavefront construction	
• Finds a new wavefront by ray tracing	• Finds a new wavefront by finite differences

REFERENCES

Audebert, F., Nichols, D. E., Rekdal, T., Biondi, B., Lumley, D. E., and Urdaneta, H., 1997, Imaging complex geologic structure with single-arrival Kirchhoff prestack depth migration: Geophysics, **62**, 1533–1543.

Červený, V., 1987, Ray tracing algorithms in three-dimensional laterally varying layered structures, *in* Nolet, G., Ed., Seismic tomography: D. Reidel Publ. Co., 99–134.

Geoltrain, S., and Brac, J., 1993, Can we image complex structures with first-arrival traveltime?: Geophysics, **58**, 564–575.

Gray, S. H., and May, W. P., 1994, Kirchhoff migration using eikonal equation traveltimes: Geophysics, **59**, 810–817.
Moser, T. J., 1991, Shortest path calculation of seismic rays: Geophysics, **56**, 59–67.
Nichols, D., Farmer, P., and Palacharla, G., 1998, Improving prestack imaging by using a new ray selection method: 68th Ann. Internat. Mtg., Soc. Expl. Geophys., Expanded Abstracts, 1546–1549.
Pereyra, V., 1992, Two-point ray tracing in general 3D media: Geophys. Prosp., **40**, 267–288.
Qin, F., Luo, Y., Olsen, K. B., Cai, W., and Schuster, G. T., 1992, Finite-difference solution of the eikonal equation along expanding wavefronts: Geophysics, **57**, 478–487.
Sethian, J., and Popovici, A. M., 1999, 3-D traveltime computation using the fast marching method: Geophysics, **64**, 516–523.
Strahilevitz, R., Kosloff, D. D., and Koren, Z., 1998, Three-dimensional two-point ray tracing using paraxial rays in Cartesian coordinates: 68th Ann. Internat. Mtg., Soc. Expl. Geophys., Expanded Abstracts, 1887–1892.
van Trier, J., and Symes, W. W., 1991, Upwind finite-difference calculation of traveltimes: Geophysics, **56**, 812–821.
Vidale, J. E., 1990, Finite-difference calculation of traveltimes in three dimensions: Geophysics, **55**, 521–526.
Vinje, V., Iversen, E., and Gjoystdal, H., 1993, Traveltime and amplitude estimation using wavefront construction: Geophysics, **58**, 1157–1166.
Zhang, L., 1993, Imaging by the wavefront propagation method: Ph.D. thesis, Stanford Univ.